Acta Cryst B
STRUCTURAL SCIENCE
CRYSTAL ENGINEERING
MATERIALS

ISSN 2052-5206

Crystal structure refinements of tetragonal (OH,F)-rich spessartine and henritermierite garnets

Sytle M. Antao* and Laura A. Cruickshank

Department of Geoscience, University of Calgary, Calgary, Alberta T2N 1N4, Canada. *Correspondence e-mail: antao@ucalgary.ca

Received 13 November 2017
Accepted 20 December 2017

Edited by S. Parsons, University of Edinburgh, Scotland

Keywords: (OH, F)-spessartine; henritermierite; garnets; ordering of anions; structure; chemistry; hydrogen bonding.

Supporting information: this article has supporting information at journals.iucr.org/b

Cubic garnet (space group $Ia\bar{3}d$) has the general formula $X_3Y_2Z_3O_{12}$, where X, Y and Z are cation sites. In the tetragonal garnet (space group $I4_1/acd$), the corresponding cation sites are $X1$ and $X2$, Y, and $Z1$ and $Z2$. In both space groups only the Y site is the same. The crystal chemistry of a tetragonal (OH,F)-rich spessartine sample from Tongbei, near Yunxiao, Fujian Province, China, with composition $^{X}(Mn_{2.82}Fe^{2+}_{0.14}Ca_{0.04})_{\Sigma3}{}^{Y}\{Al_{1.95}Fe^{3+}_{0.05}\}_{\Sigma2}{}^{Z}[(SiO_4)_{2.61}(O_4H_4)_{0.28}(F_4)_{0.11}]_{\Sigma3}$ ($Sps_{94}Alm_5Grs_1$) was studied with single-crystal X-ray diffraction and space group $I4_1/acd$. The deviation of the unit-cell parameters from cubic symmetry is small [a = 11.64463 (1), c = 11.65481 (2) Å, c/a = 1.0009]. Point analyses and back-scattered electron images, obtained by electron-probe microanalysis, indicate a homogeneous composition. The $Z2$ site is fully occupied, but the $Z1$ site contains vacancies. The occupied $Z1$ and $Z2$ sites with Si atoms are surrounded by four O atoms, as in anhydrous cubic garnets. Pairs of split sites are O1 with F11 and O2 with O22. When the $Z1$ site is vacant, a larger $[(O_2H_2)F_2]$ tetrahedron is formed by two OH and two F anions in the O22 and F11 sites, respectively. This $[(O_2H_2)F_2]$ tetrahedron is similar to the O_4H_4 tetrahedron in hydrogarnets. These results indicate $^{X}Mn^{2+}_3{}^{Y}Al_2{}^{Z}[(SiO_4)_2(O_2H_2)_{0.5}(F_2)_{0.5}]_{\Sigma3}$ as a possible end member, which is yet unknown. The H atom that is bonded to the O22 site is not located because of the small number of OH groups. In contrast, tetragonal henritermierite, ideally $^{X}Ca_3{}^{Y}Mn^{3+}_2{}^{Z}[(SiO_4)_2(O_4H_4)_1]_{\Sigma3}$, has a vacant $Z2$ site that contains the O_4H_4 tetrahedron. The H atom is bonded to an O3 atom [O3—H3 = 0.73 (2) Å]. Because of O2—Mn^{3+}—O2 Jahn–Teller elongation of the $Mn^{3+}O_6$ octahedron, a weak hydrogen bond is formed to the under-bonded O2 atom. This causes a large deviation from cubic symmetry (c/a = 0.9534).

1. Introduction

Most common garnet-group minerals with the general formula, $^{[8]}X_3{}^{[6]}Y_2{}^{[4]}Z_3{}^{[4]}O_{12}$, Z = 8, exhibit cubic symmetry with space group $Ia\bar{3}d$, but there are a few rare members that crystallize in the tetragonal space group $I4_1/acd$. Examples of common cubic garnets are pyrope (Prp), almandine (Alm), and spessartine (Sps) that make up the pyralspite series with the formula, $(Mg,Fe,Mn)_3Al_2[SiO_4]_3$, whereas grossular (Grs), uvarovite (Uv), and andradite (Adr) make up the ugrandite series, $Ca_3\{Al,Cr,Fe\}_2[SiO_4]_3$. Based on O_4H_4 substitution for SiO_4, cubic hydrogarnets are common in the ungrandite series with the general formula $Ca_3\{Al,Cr,Fe\}_2[(SiO_4)_{3-x}(O_4H_4)_x]_{\Sigma3}$ [see Antao (2015), and references therein]. Such hydrogarnet substitutions are rare and occur to a limited extent in the pyralspite series. The H-atom positions in some of these cubic hydrogarnets were located and refined.

The eight-coordinated dodecahedral X site in cubic garnet contains Mg^{2+}, Fe^{2+}, Mn^{2+} or Ca^{2+} cations, the six-coordinated

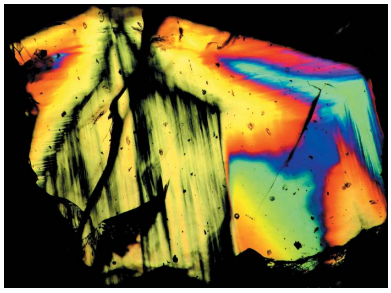

octahedral *Y* site contains Al^{3+}, Cr^{3+}, Fe^{3+}, Mn^{3+}, Ti^{4+} or Zr^{4+} cations, and the four-coordinated tetrahedral *Z* site contains Si^{4+} or Fe^{3+} cations, or (O_4H_4) groups (Armbruster, 1995; Novak & Gibbs, 1971; Ungaretti *et al.*, 1995; Antao & Cruickshank, 2016; Antao, 2013*b*). The garnet structure consists of alternating ZO_4 tetrahedra and YO_6 octahedra with *X* atoms forming XO_8 dodecahedra. The eight O atoms in the XO_8 dodecahedron occur at the corners of a distorted cube. Each O atom is four-coordinated tetrahedrally by two *X*, one *Y* and one *Z* cation. The O atom is on a general position and the cation positions are fixed in cubic garnets.

There are three rare hydrogarnet minerals with tetragonal space group $I4_1/acd$: (OH,F)-rich spessartine, ideally $Mn_3^{2+}Al_2[(SiO_4)_2(O_4H_4,F_4)_1]_{\Sigma3}$ (Boiocchi *et al.*, 2012); henritermierite, ideally $Ca_3Mn_2^{3+}[(SiO_4)_2(O_4H_4)_1]_{\Sigma3}$ (Armbruster *et al.*, 2001; Aubry *et al.*, 1969); and holtstamite, ideally $Ca_3(Al,Mn^{3+})_2[(SiO_4)_2(O_4H_4)_1]_{\Sigma3}$ with Al > Mn (Hålenius *et al.*, 2005). The name spessartine is derived from the Spessart Mountains, Germany, and henritermierite is named in honour of the French geologist Henri Termier. The crystal structure of an F-bearing spessartine was refined in space group $Ia\bar{3}d$ (Smyth *et al.*, 1990). The lowering from cubic to tetragonal symmetry arises from Jahn–Teller distortion of the Mn^{3+} cation in the *Y* octahedral site in henritermierite. The H-atom position was located and refined only in henritermierite (Fig. 1). The F atom or OH group was not previously located in (OH,F)-spessartine.

Birefringence in cubic garnets was reported over a century ago (*e.g.* Brewster, 1853; Mallard, 1876), but the origin remains questionable. Some almandine, grossular, spessartine, andradite, uvarovite and hydrogarnet samples are anisotropic under cross-polarized light, which may indicate that they are not optically cubic (Allen & Buseck, 1988; Brown & Mason, 1994; Deer *et al.*, 1982; Rossman & Aines, 1991). Several reasons have been given for the birefringence, but the main one appears to be cation order in the *X* and *Y* sites that cause a symmetry reduction (Akizuki, 1984; Allen & Buseck, 1988; Frank-Kamenetskaya *et al.*, 2007; Takéuchi *et al.*, 1982). Other suggested reasons for the birefringence in garnet were discussed elsewhere and are not repeated here (Antao & Klincker, 2013).

Majorite garnet, $(Mg,Fe)SiO_3$, is considered to be a major constituent of the Earth's transition zone between the 400- and 670-km discontinuities (Akaogi & Akimoto, 1977; Ito & Takahashi, 1987; Liu, 1977; Ringwood, 1967). End-member anisotropic majorite $MgSiO_3$, that is $\{Mg_3\}(MgSi)[Si_3O_{12}]$ in analogy with cubic garnets, was reported to be birefringent with tetragonal symmetry (Angel *et al.*, 1989; Kato & Kumazawa, 1985; Nakatsuka *et al.*, 1999; Nakatsuka, Yoshiasa, Yamanaka, Ohtaka *et al.*, 1999; Parise *et al.*, 1996; Sawamoto, 1987). Similarly, other ABO_3-related tetragonal phases such as $CaGeO_3$, $CdGeO_3$ (Nakatsuka, 2005; Prewitt & Sleight, 1969), and $MnSiO_3$ (Fujino *et al.*, 1986) contain an equal number of *A* and *B* atoms on the *Y* site. If cation order and cubic symmetry reduction occur for birefringent ABO_3 garnet, then their thermodynamic properties will change. For example, the configurational entropy for an ordered tetragonal ABO_3 garnet would change relative to a disordered cubic phase, and gives rise to a change in enthalpy. Therefore, it is important to know the correct symmetry of garnets. In the case of pyrope–majorite solid solutions, it was shown that near-end member majorite is, in fact, cubic (Antao, Suarez Nieto *et al.*, 2015).

Many garnets are single cubic phases, especially those in the pyrope–almandine series (Antao, 2014*b*; Antao *et al.*, 2014). Several studies have observed birefringent garnets with lamellar or oscillatory features, which were referred to as 'chemical zoning' instead of separate phases (*e.g.* Akizuki, 1984; Ivanova *et al.*, 1998; Jamtveit, 1991; Pollok *et al.*, 2001). Such birefringent garnets contain two or three cubic phases that are easily observed with powder X-ray diffraction techniques using either a synchrotron or a laboratory X-ray source (*e.g.* Antao, 2013*b*,*c*; Schingaro *et al.*, 2016). In contrast to these interpretations, birefringence in majorite garnet was attributed to a lower symmetry phase that forms by a transition from a cubic phase (*e.g.* Hatch & Ghose, 1989; Hatch &

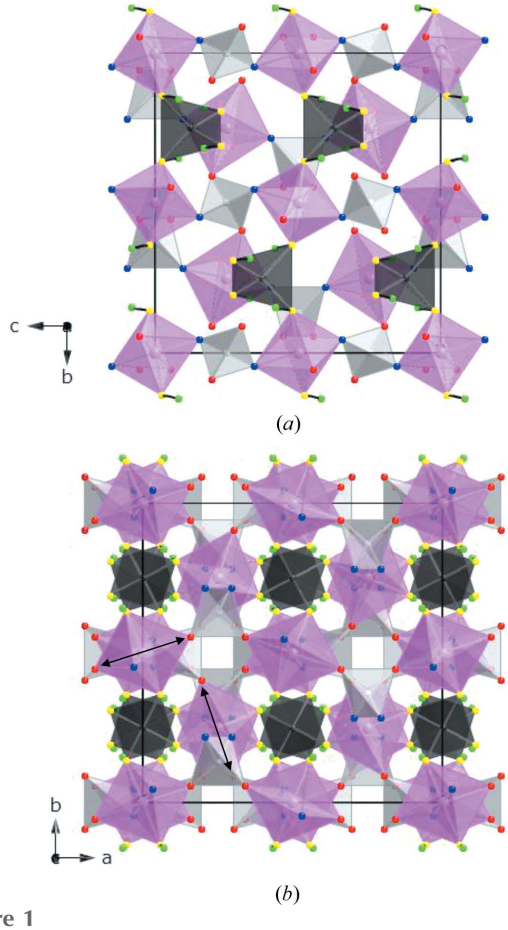

Figure 1
Tetragonal henritermierite structure showing the linkages of the *Y* octahedra (pink), *Z*1 (light grey) and *Z*2 (dark grey) tetrahedra. The H atoms (green) are bonded to O3 atoms (yellow) when the *Z*2 site is vacant. The O1 (blue) and O2 (red) atoms are shown. The *X*1 and *X*2 dodecahedral sites are omitted for clarity. (*a*) When a slice of the structure is viewed down [100], the O—H bonds are clearly observed. The H sites are slightly above the *Z*2 tetrahedral faces. (*b*) When the structure is viewed down [001], open channels parallel to the *c* axis occur where the *Z*2 site is vacant. Because the O2—Mn^{3+}—O2 Jahn–Teller octahedral elongations are sub-parallel to the *a* and *b* axes, *c*/*a* = 0.953, so the deviation from cubic symmetry is large (double-headed arrows).

Griffen, 1989). Diffraction peaks from garnets showing split reflections were observed (*e.g.* Bank, 1982; Hirai & Nakazawa, 1986*b*,*a*; Koritnig *et al.*, 1978; Manning & Owens, 1977; Zabinski, 1966). Recently, multiphase intergrowths of two or three cubic garnet phases also show split reflections (*e.g.* Antao, 2013*b*,*a*,*c*; Antao & Round, 2014; Antao, Zaman *et al.*, 2015; Schingaro *et al.*, 2016; Antao, 2014*a*; Antao & Klincker, 2014; Antao, Mohib *et al.*, 2015).

Using the Rietveld method and synchrotron high-resolution powder X-ray diffraction (HRPXRD) data, this study excludes the possibility that (OH,F)-spessartine or henritermierite contains two cubic phases. Because these samples contain a single tetragonal phase, a single-crystal X-ray diffraction (SCXRD) study was carried out with space group $I4_1/acd$ to locate the F and OH anions. The H-atom position was not located in (OH,F)-spessartine, but it was easily located and refined for henritermierite.

2. Sample description

The (OH,F)-spessartine sample is from Tongbei, near Yunxiao, Fujian Province, China. The specimen contains numerous crystals of size 1–3 mm that are transparent and orange in colour. Under cross-polarized light, the crystals are birefringent and contain some lamellar features (Fig. 2). However, the plane-polarized light and back-scattered electron (BSE) images (not shown) show no inhomogeneous features.

The henritermierite sample is from Wessels Mine X, Kalahari Manganese Field, North Cape, South Africa. This sample was obtained from the Royal Ontario Museum (ROM #M54234). The orange henritermierite garnet is associated with hausmannite spinel, $Mn^{2+}Mn_2^{3+}O_4$.

3. Analytical methods

3.1. Electron-probe microanalyzer

Quantitative chemical compositions and back-scattered electron (BSE) images were obtained with a Jeol JXA-8200 WD-ED electron-probe microanalyzer (EPMA). The Jeol operating program on a Solaris platform was used for ZAF correction and data reduction. The wavelength-dispersive operating conditions were 15 kV accelerating voltage, 20 nA beam current and 5 µm beam diameter. The following standards were used: almandine–pyrope (Mg $K\alpha$), grossular (Ca $K\alpha$), almandine (Fe $K\alpha$, Al $K\alpha$, Si $K\alpha$), rutile (Ti $K\alpha$), spessartine (Mn $K\alpha$), chromite (Cr $K\alpha$) and fluorapatite (F $K\alpha$).

In this study, fragments from a large single crystal of (OH,F)-spessartine ($\simeq$ 3 mm in diameter) were examined using various techniques. The fragments are chemically homogeneous. The Fe^{3+}/Fe^{2+} cations were distributed between the X and Y sites based on garnet 3:2:3 stoichiometry, full site

Table 1
EPMA results for (OH,F)-rich spessartine and henritermierite garnets.

The EPMA formulae are: (1) $(Mn_{2.82}Fe^{2+}_{0.14}Ca_{0.04})_{\Sigma3}\{Al_{1.95}Fe^{3+}_{0.05}\}_{\Sigma2}[(SiO_4)_{2.61}(O_4H_4)_{0.28}(F_4)_{0.11}]_{\Sigma3}$; $Sps_{94}Alm_5Grs_1$ (this study). (2) $(Mn_{2.87}Fe_{0.09}Ca_{0.04})_{\Sigma3}\{Al_{1.94}Fe_{0.06}\}_{\Sigma2}[(SiO_4)_{2.52}(O_4H_4)_{0.28}(F_4)_{0.20}]_{\Sigma3}$; $Sps_{96}Alm_3Grs_1$ (Boiocchi *et al.*, 2012). (3) $(Mn_{2.67}Fe_{0.33}Ca_{0.05})_{\Sigma3.06}\{Al_{1.97}Ti_{0.01}\}_{\Sigma1.98}[(SiO_4)_{2.70}(O_4H_4)_{0.09}(F_4)_{0.24}]_{\Sigma3.04}$; $Sps_{87}Alm_{11}Grs_2$ (Smyth *et al.*, 1990). (4) $Ca_{3.00}\{Mn_{1.94}Al_{0.04}Fe_{0.02}\}_{\Sigma2}[(SiO_4)_{1.98}(O_4H_4)_{1.02}]_{\Sigma3}$ (this study). (5) $(Ca_{2.98}Mg_{0.01}Na_{0.01})_{\Sigma3}\{Mn_{1.95}Al_{0.05}Fe_{0.01}\}_{\Sigma2}[(SiO_4)_{2.07}(O_4H_4)_{0.93}]_{\Sigma3}$ (Armbruster *et al.*, 2001).

	(OH,F)-rich spessartine			Henritermierite	
	(1)	(2)	(3)	(4)	(5)
SiO_2 (wt%)	32.04	31.32	32.55	24.64	26.22
TiO_2	0.06	0.05	0.06	–	–
Al_2O_3	20.33	20.47	20.13	0.41	0.48
FeO	2.08	1.33	4.79	–	–
Fe_2O_3	0.74	0.99	0.00	0.33	0.14
MnO	40.83	42.20	37.98	–	–
Mn_2O_3	–	–	–	31.69	32.36
MgO	0.02	0.01	0.00	0.01	0.09
CaO	0.46	0.46	0.60	34.77	35.20
Na_2O	–	–	–	0.00	0.06
(H_2O)†	2.08	2.10	0.64	7.57	5.46
F	1.78	3.21	3.68	–	–
$-O\equiv F$	0.75	1.35	1.55	–	–
$\sum$	99.64	100.79	98.88	99.41	100.01
Mn^{2+} apfu	2.815	2.870	2.673	–	–
Fe^{2+}	0.141	0.089	0.333	–	–
Ca^{2+}	0.040	0.040	0.053	2.999	2.981
Mg^{2+}	0.003	0.001	0.000	0.001	0.011
Na	–	–	–	0.000	0.009
$\sum X$	3.000	3.000	3.059	3.000	3.001
Al^{3+}	1.951	1.937	1.970	0.039	0.045
Mn^{3+}	–	–	–	1.942	1.947
Fe^{3+}	0.045	0.060	0.000	0.020	0.008
Ti^{4+}	0.004	0.003	0.007	–	–
$\sum Y$	2.000	2.000	1.977	2.001	2.000
Si^{4+}	2.609	2.515	2.704	1.983	2.072
H_4	0.277	0.204	0.089	1.017	0.928
F_4	0.114	0.281	0.242	–	–
$\sum Z$ = [Si +(OH,F)/4]	3.000	3.000	3.035	3.000	3.000
X EPMA	74.88	74.87	76.54	59.99	59.85
Y	26.62	26.80	25.76	49.58	49.47
Z	36.53	35.21	37.86	31.73	33.15
X SCXRD	75.00	75.20	75.00	60.00	60.00
Y	26.00	26.39	26.00	49.28	50.00
Z	35.98	36.37	37.80	28.28	28.98
ΔX‡	0.1	0.3	−1.5	0.0	0.1
ΔY	−0.6	−0.4	0.2	−0.3	0.5
ΔZ	−0.6	1.2	−0.1	−3.5	−4.2

† H_2O was calculated from Si + (OH,F)/4 = 3. ‡ Δ is the difference in electrons between SCXRD structure refinement results and EPMA site values.

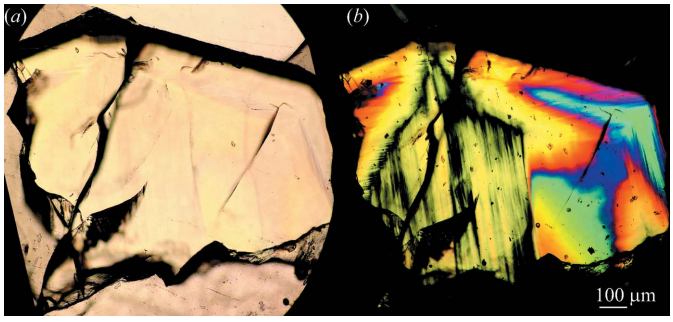

Figure 2
(*a*) Plane-polarized light (PPL) and (*b*) cross-polarized light (XPL) images from a 80 µm-thick section of (OH,F)-spessartine. The XPL images shows birefringence and some lamellar features, but the PPL and BSE images (in particular, the BSE image that is not shown) do not show any significant inhomogeneous features

occupancies and charge neutrality. The H_2O content was calculated based on Si + (OH,F)/4 = 3. The oxide wt% and atoms per formula unit (apfu) are reported (Table 1). The composition of the sample is similar to that reported for other (OH,F)-spessartine samples (Table 1). A comparison between the SCXRD structure refinement results and EPMA site-scattering values is given in Table 1. In a similar manner, the henritermierite sample was analyzed and the composition is given (Table 1).

3.2. FTIR spectroscopy

At room temperature, 32 infrared scans were collected on a Nicolet Nexus 470 FTIR (Thermo Fisher Scientific Inc.) spectrometer operating at 2 cm^{-1} resolution for the (OH,F)-spessartine sample only. The powdered sample (the same batch that was used for the HRPXRD experiment below) was mixed with KBr and pressed into a disc for measurements. Infrared absorption spectra in the 3400–3800 cm^{-1} region are displayed (Fig. 3). This spectrum is a summation of the 32 scans and the O—H stretching region shown is of importance. Two prominent bands are observed: the intense band is centred at 3577 cm^{-1} and the other less intense band consists of an unresolved doublet at 3631 and 3621 cm^{-1}. These bands indicate a hydrous (OH) component and are similar to those observed by Smyth *et al.* (1990) and Boiocchi *et al.* (2012). The FTIR spectrum suggests three different OH environments.

3.3. Synchrotron high-resolution powder X-ray diffraction

Both samples were studied using HRPXRD at beamline 11-BM, Advanced Photon Source, Argonne National Laboratory. A small fragment (about 2 mm in diameter) of each sample was crushed under methanol to a fine powder using a corundum mortar and pestle. The crushed sample was loaded into a Kapton capillary (0.8 mm internal diameter) and rotated during the experiment at a rate of 90 rotations per second. The data were collected at 296 K to a maximum 2θ of ~50° with a step size of 0.001° and a step time of 0.1 seconds per step. The HRPXRD pattern was collected with a unique multi-analyzer detection assembly consisting of 12 independent silicon (111) crystal analyzers and $LaCl_3$ scintillation detectors that reduce the angular range to be scanned and allow rapid acquisition of data. Silicon (NIST 640c) and alumina (NIST 676a) standards (ratio of $\frac{1}{3}Si{:}\frac{2}{3}Al_2O_3$ by weight) were used to calibrate the instrument and refine the monochromatic wavelength used in the experiment (Table 2). Additional details of the experimental set-up are given elsewhere (Lee *et al.*, 2008; Wang *et al.*, 2008). Similar experiments have been used to examine other minerals (*e.g.* Antao *et al.*, 2002; Antao & Hassan, 2002; Ehm *et al.*, 2007; Skinner *et al.*, 2011; Moyer *et al.*, 2008).

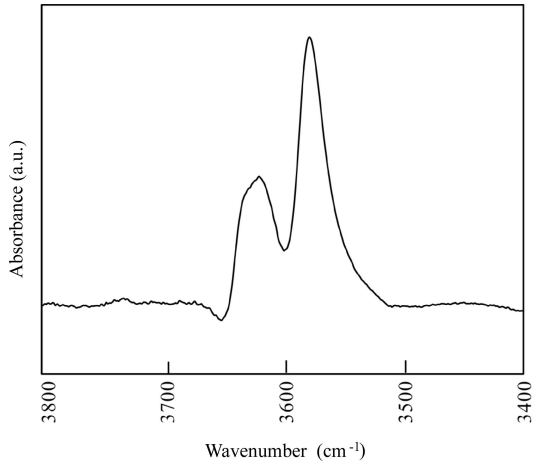

Figure 3
FTIR spectra for tetragonal (OH,F)-spessartine showing two prominent bands corresponding to OH groups: one band is centred at 3577 cm^{-1} and the other band consists of a doublet at 3631 and 3621 cm^{-1}.

Table 2
HRPXRD data and Rietveld refinement statistical indicators.

	(OH,F)-rich spessartine (1)	Henritermierite (4)
a (Å)	11.64463 (1)	12.49075 (5)
c (Å)	11.65481 (2)	11.90921 (5)
c/a	1.0009	0.95344
V (Å^3)	1580.361 (4)	1858.06 (1)
Reduced χ^2	1.771	4.570
$R(F^2)$†	0.0403	0.0693
wRp	0.0631	0.1398
N_{obs}	1827	2215
λ (Å)	0.41383 (2)	0.41374 (2)
Data points	47 992	47 995

† $R(F^2)$ = overall R-structure factor based on observed and calculated structure amplitudes = $[\sum(F_o^2 - F_c^2)/\sum(F_o^2)]^{1/2}$. 2θ range = 2–50°.

3.4. Rietveld structure refinements

The HRPXRD data were analyzed with the Rietveld method (Rietveld, 1969) as implemented in the *GSAS* package (Larson & Von Dreele, 2000) and using the *EXPGUI* graphical interface (Toby, 2001) of that package. Scattering curves for neutral atoms were used. The unit-cell parameters were refined using the HRPXRD data. The atom coordinates and space group, $I4_1/acd$, were taken from our single-crystal results and these were held constant. The background was modelled with a shifted Chebyschev polynomial (six terms). The reflection-peak profiles were fitted using type-3 profile (pseudo-Voigt; Caglioti *et al.*, 1958; Thompson *et al.*, 1987). Examination of the HRPXRD pattern for (OH,F)-spessartine shows a single tetragonal phase instead of the multiple cubic phases that were observed for other birefringent cubic garnets. No impurities or unindexed peaks were observed (Fig. 4). The HRPXRD data for henritermierite were analyzed in a similar manner. The unit-cell parameters, Rietveld refinement statistical indicators, and fitting parameters are given (Table 2). The structures will be discussed using the single-crystal results. The Rietveld unit-cell parameters from Table 2 were used in the single-crystal structure refinements because they are more accurate.

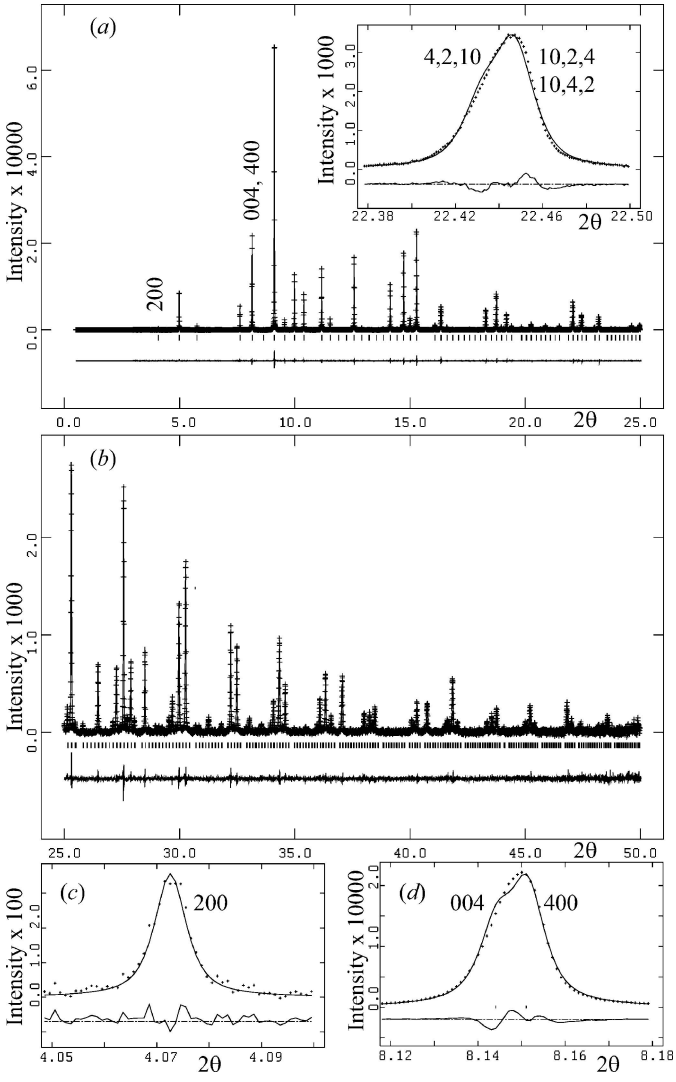

Figure 4
Complete HRPXRD pattern for tetragonal (OH,F)-spessartine (*a*) 0–25°, and (*b*) 25–50° 2θ range. The difference curve ($I_{obs} - I_{calc}$) is shown at the bottom. Short vertical lines indicate allowed reflection positions. Expanded scales of (*c*) 200 and (*d*) 004 and 400 reflections that occur at low 2θ values are also given. The separation or splitting of the 004 and 400 reflections is often used to indicate tetragonal symmetry. This splitting may also arise from two slightly different cubic phases (see text). The 200 reflection confirms the tetragonal symmetry. The splitting of a high-angle reflection is shown as an insert in (*a*).

3.5. Single-crystal X-ray diffraction

Single-crystal X-ray diffraction (SCXRD) data were collected at 296 (2) K with a Nonius Kappa CCD on a Bruker–Nonius FR591 rotating anode diffractometer with graphite-monochromated Mo $K\alpha$ radiation. The generator setting was 50 kV and 36 mA. The detector-to-crystal distance was fixed at 35 mm. A total of ten frames were collected for unit-cell determination. The scan settings were 1° rotation per frame (total rotation = 10°) and 22 seconds X-ray exposure time per frame. After obtaining satisfactory unit-cell parameters and mosaicity values (less than 1°), a complete data set was collected using a 2° per frame rotation with exposure of 42–122 seconds per frame. The diffraction spots were measured in full, scaled with *SCALEPACK*, corrected for Lorentz–polarization and integrated using the Nonius program suite *DENZO-SMN* (Otwinowski & Minor, 1997). The space group $I4_1/acd$ was obtained based on systematic absences and structure factor statistics. Full-matrix least-squares refinements were carried out with the *SHELXL* program using neutral atom scattering factors (Sheldrick, 2015) running under *WinGX* (Farrugia, 2012). For (OH,F)-spessartine, the starting structural model was that used by Boiocchi *et al.* (2012). For henritermierite, the starting structural model was from Armbruster *et al.* (2001). Anisotropic displacement parameters were used for all the atoms in (OH,F)-spessartine. For henritermierite, only the Si2 and H3 sites were refined using isotropic displacement parameters. For the SCXRD structure refinements of both (OH,F)-spessartine and henritermierite, the site occupancy factors (s.o.f.s) were refined together with the isotropic displacement parameters for each atom site. After all the s.o.f.s were obtained in this manner, they were then fixed while the anisotropic displacement parameters were refined. Details of the data collection, processing and refinement are given in Table 3. The atom coordinates, s.o.f.s and equivalent isotropic displacement parameters are given in Table 4. Anisotropic displacement parameters are given in Table 5. Selected bond distances and angles are given in Table 6. Bond-valence sums (BVS) are given in Table 7.

4. Discussion

4.1. Crystal structure of (OH,F)-spessartine

The chemical formula obtained using the EPMA for the (OH,F)-spessartine sample is $^{X}(Mn_{2.82}Fe^{2+}_{0.14}Ca_{0.04})_{\Sigma3}$-$^{Y}\{Al_{1.95}Fe^{3+}_{0.05}\}_{\Sigma2}{}^{Z}[(SiO_4)_{2.61}(O_4H_4)_{0.28}(F_4)_{0.11}]_{\Sigma3}$ (Table 1). The corresponding formula from the SCXRD structure refinement is $^{X}Mn_3{}^{Y}Al_2{}^{Z}[(SiO_4)_{2.61}(O_4H_4)_{0.23}(F_4)_{0.15}]_{\Sigma3}$ [Table 4(*a*)]. There are Z (= Si) cation vacancies. Using all the atoms obtained by the EPMA, s.o.f.s were calculated in terms of the dominant atoms in the X(Mn), Y(Al) and Z(Si) sites, and then converted to electrons. The agreement between EPMA and SCXRD structure refinement results, in terms of electrons, is reasonable (Table 1).

The complete HRPXRD pattern for the (OH,F)-spessartine sample is given in Fig. 4. The expanded patterns show that the 200 reflection peak is a single peak (Fig. 4*c*), but the 004 and 400 reflections occur as split peaks because of the tetragonal symmetry (Fig. 4*d*). The separation or splitting of the 004 and 400 cubic reflections is sometimes used to indicate tetragonal symmetry in garnets (Heinemann *et al.*, 1997; Parise *et al.*, 1996). However, this splitting may also arise from two cubic phases (*e.g.* Antao, 2013*a*,*c*; Antao & Hassan, 2010).

The 200 reflection is absent in cubic spessartine (Fig. 5*a*), weak in tetragonal (OH,F)-spessartine (Fig. 5*b*), and is much stronger in henritermierite (Fig. 5*c*). Therefore, the 200 reflection may be used to distinguish between tetragonal and cubic garnets. The $h00$: $h = 4n$ condition of space group $Ia\bar{3}d$ is violated for both $h00$ and $0k0$ reflections as can be seen from

Table 3
SCXRD data.

(*a*) (OH,F)-rich spessartine†

	This study (1)	Boiocchi *et al.* (2012) (2)
Chemical formula	$Mn_3Al_2[(SiO_4)_{2.61}(O_4H_4)_{0.23}(F_4)_{0.15}]_{\Sigma 3}$	
Unit-cell dimensions (Å)	$a = b = 11.6446$ (2), $c = 11.6548$ (2)	$a = b = 11.6347$ (3), $c = 11.6449$ (3)
c/a	1.0009	1.0009
Volume (Å^3)	1580.35 (5)	1576.3 (1)
a (pseudo cubic) (Å)	11.648	11.638
Density (calc.) (Mg m^{-3})	4.076	4.085
Absorption coefficient (mm^{-1})	5.43	
$F(000)$	1869	
Crystal size (mm)	0.07 × 0.08 × 0.09	0.15 × 0.30 × 0.42
θ range (°)	4.28–62.81	1–55
No. of reflections collected	50 335	24 602
No. of independent reflections	3235 ($R_{int} = 0.0364$)	2473 ($R_{int} = 0.0360$)
No. of observed reflections [$I > 2\sigma(I)$]	2665	
$(\sin\theta/\lambda)_{max}$ (Å^{-1})	1.252	
Refinement method	Full-matrix least-squares on F^2	
No. of data, restraints, parameters	3235, 0, 67	
S (goodness-of-fit on F^2)	1.232	
Final R indices [$F^2 > 2\sigma(F^2)$]	$R_1 = 0.0290$, $wR_2 = 0.0743$	
R indices (all data)	$R_1 = 0.0387$, $wR_2 = 0.0775$	$R_1 = 0.0314$
$\Delta\rho_{max}$ (e Å^{-3})	0.68 (0.40 Å from O3)	0.83
$\Delta\rho_{min}$ (e Å^{-3})	−1.65 (0.00 Å from Si2)	

(*b*) Henritermierite†

	This study (4)	Armbruster *et al.* (2001) (5)
Chemical formula	$Ca_3(Mn_{1.94}Al_{0.06})[(SiO_4)_{2.02}(O_4H_4)_1]_{\Sigma 3}$	
Unit-cell dimensions (Å)	$a = b = 12.4908$ (2), $c = 11.9092$ (2)	$a = b = 12.489$ (1), $c = 11.909$ (1)
c/a	0.9534	0.9536
Volume (Å^3)	1858.07 (5)	1857.5
a (pseudo cubic) (Å)	12.2938	12.293
Density (calc.) (Mg m^{-3})	3.4431	
Absorption coefficient (mm^{-1})	4.63	
$F(000)$	1901	
Crystal size (mm)	0.05 × 0.05 × 0.06	0.1 × 0.2 × 0.18
θ range (°)	4.13–39.98	≤ 40
No. of reflections collected	17 620	4235
No. of independent reflections	1401 ($R_{int} = 0.0294$)	1167
No. of observed reflections [$I > 2\sigma(I)$]	1340	
$(\sin\theta/\lambda)_{max}$ (Å^{-1})	0.904	
Refinement method	Full-matrix least-squares on F^2	
No. of data, restraints, parameters	1401, 0, 52	
S (goodness-of-fit on F^2)	1.209	1.224
Final R indices [$F^2 > 2\sigma(F^2)$]	$R_1 = 0.0204$, $wR_2 = 0.0428$	$R_1 = 0.0162$, $wR_2 = 0.0390$
R indices (all data)	$R_1 = 0.0227$, $wR_2 = 0.0432$	
$\Delta\rho_{max}$ (e Å^{-3})	0.44 (0.80 Å from O1)	
$\Delta\rho_{min}$ (e Å^{-3})	−1.36 (0.00 Å from Mn)	

† Temperature = 296 (2) K, λ (Mo $K\alpha$) = 0.71073 Å, $Z = 8$, tetragonal, space group $I4_1/acd$.

the 200 reflection (Fig. 5). Henritermierite contains many more reflections that violate cubic symmetry. The tetragonal unit-cell parameters for (OH,F)-spessartine deviate slightly from cubic symmetry [$c/a = 1.0009$; Table 3(*a*)]. However, this deviation is large in henritermierite [$c/a = 0.9534$; Table 3(*b*)].

Our bond distances and angles are similar to those obtained by Boiocchi *et al.* (2012), but there are significant differences [Table 6(*a*)]. The two XO_8 dodecahedra or distorted cubes have similar average ⟨Mn1—O⟩ = 2.338 (1) Å and average ⟨Mn2—O⟩ = 2.335 (1) Å distances [Table 6(*a*)]. Smyth *et al.* (1990) obtained ⟨X—O⟩ = 2.319 (1) Å in their cubic structure refinement. Tetragonal and cubic spessartine samples have average ⟨$X1,X2$—O⟩ and ⟨X—O⟩ distances that are nearly equal to each other [Table 6(*a*)]. The YO_6 octahedron has an average ⟨Al—O⟩ distance of 1.902 (1) Å, which is similar to that in cubic spessartine [1.8956 (4) Å; Table 6(*a*)].

The $Z1$ site contains some vacancies, but the $Z2$ site is fully occupied [Table 4(*a*)]. The O3 site is fully occupied, in contrast with the results of Boiocchi *et al.* (2012) and that for henritermierite (Armbruster *et al.* 2001) where the O3 position was split between O3 and a nearby O33 position (corresponding to O3′ or O3*A* in the previous studies). However, the other two O atom positions are split into O1 and F11 positions and O2 and O22 split positions (Fig. 6*a*). The F11 site contains F atoms and the O22 site contains O atoms from the OH groups. These split positions are used to describe the three environments that contain O, OH, and F anions [Figs. 6(*a*) and 6(*b*)].

Because of the size of the anions [F^- (1.31 Å), OH^- (1.35 Å), and O^{2-} (1.38 Å)], the $Z1$—F11 distance is the largest [1.878 (5) Å], average ⟨$Z1$—O⟩ is smallest [1.639 (1) Å], and the $Z1$—O22 is intermediate in size [1.815 (6) Å; Table 6(*a*)]. The large distances arise from OH and F anion substitution for O atoms. The large distances arise from anion–anion repulsions when the $Z1$ site is vacant, whereas the short distance indicates that the $Z1$ site is occupied with Si atoms.

The $Z1$ and $Z2$ sites are in tetrahedral coordination. The vacant Z site is expected to have a large average ⟨Z—O⟩ distance. This is not the case with the average ⟨$Z1$—O⟩ = 1.639 (1) Å and $Z2$—O3 = 1.6427 (4) Å, so both distances are nearly the same and these are similar to that in anhydrous cubic spessartine [1.6416 (4) Å; Table 6(*a*)] with no significant Si-atom vacancies (Antao & Round, 2014; Merli *et al.*, 1995; Novak & Gibbs, 1971). Boiocchi *et al.* (2012) obtained ⟨$Z1$—O⟩ = 1.644 (1) Å and ⟨$Z2$—O3⟩ = 1.634 (1) Å, which is a significant difference from the results in this study. When the $Z1$ site is vacant, the tetrahedron is made up of O_2H_2 and F_2 (Fig. 6*a*), so the $Z1$–O22 and $Z1$—F11 distances are quite large with average ⟨$Z1$—

Table 4
Atom coordinates, equivalent isotropic displacement parameters and s.o.f.s.

The chemical formula obtained by refinement is: $Mn_3Al_2[(SiO_4)_{2.61}(O_4H_4)_{0.23}(F_4)_{0.15}]_{\Sigma3}$ for (1) and $Ca_3(Mn_{1.94}Al_{0.06})[(SiO_4)_{2.02}(O_4H_4)_1]_{\Sigma3}$ for (4). In spessartine (1), O1 and F11 constitute one split position, whereas O2 and O22 constitute another split position. The F11 site contains F atoms and the O22 site contains O atoms from the OH groups. U_{eq} is defined as one third of the trace of the orthogonalized U_{ij} tensor.

(*a*) (OH,F)-rich spessartine (1)							
	Site	s.o.f.s	apfu	*x*	*y*	*z*	U_{eq} (Å^2)
Mn1 = *X*1	16*e*	1.0	2 Mn	0.3754 (1)	0	1/4	0.008 (1)
Mn2 = *X*2	8*b*	1.0	1 Mn	0	1/4	1/8	0.008 (1)
Al = *Y*	16*c*	1.0	2 Al	0	0	0	0.005 (1)
Si1 = *Z*1	16*e*	0.820 (4)	1.64 Si + 0.36 □	0.1255 (1)	0	1/4	0.004 (1)
Si2 = *Z*2	8*a*	0.972 (5)	0.97 Si + 0.03 □	1/2	1/4	1/8	0.005 (1)
O1	32*g*	0.851 (4)	3.40 O + 0.60 □	0.2979 (1)	0.7143 (1)	0.0977 (1)	0.006 (1)
O2	32*g*	0.77 (8)	3.08 O + 0.92 □	0.1523 (3)	0.5356 (2)	0.0471 (2)	0.006 (1)
O3	32*g*	1.0	4 O	0.4526 (1)	0.3480 (1)	0.0354 (1)	0.007 (1)
F11	32*g*	0.149 (4)	0.60 F or 0.15 F_4	0.3069 (7)	0.7319 (6)	0.1058 (6)	0.010 (1)
O22	32*g*	0.23 (8)	0.92 O or 0.23(O_4)	0.1470 (9)	0.5206 (6)	0.0537 (8)	0.007 (1)
(*b*) Henritermierite (4)							
Ca1 = *X*1	16*e*	1.0	2 Ca	0.3617 (1)	0	1/4	0.007 (1)
Ca2 = *X*2	8*b*	1.0	1 Ca	0	1/4	1/8	0.009 (1)
Mn = *Y*	16*c*	0.970 (4)†	1.94 Mn^{3+} + 0.06 Al	0	0	0	0.006 (1)
Si1 = *Z*1	16*e*	1.0	2 Si	0.1159 (1)	0	1/4	0.005 (1)
Si2 = *Z*2	8*a*	0.006 (5)	0.02 Si + 0.98 □	1/2	1/4	1/8	0.012 (3)
O1	32*g*	1.0	4 O	0.2948 (1)	0.7184 (1)	0.0966 (1)	0.008 (1)
O2	32*g*	1.0	4 O	0.1599 (1)	0.5549 (1)	0.0538 (1)	0.008 (1)
O3	32*g*	1.0	4 O or 1 O_4	0.4429 (1)	0.3599 (1)	0.0216 (1)	0.009 (1)
H3	32*g*	1.0	4 H or 1 H_4	0.4292 (16)	0.3520 (17)	0.0806 (19)	0.042 (5)

† Henritermierite (4) contains 0.030 (4) Al. The O3 s.o.f. refined to full occupancy, so the H3 site is fully occupied and Si2 is vacant within error.

Table 5
Anisotropic displacement parameters (Å^2).

The anisotropic displacement factor exponent takes the form: $-2\pi^2(h^2a^{*2}U_{11} + ... + 2hka^*b^*U_{12})$.

(*a*) (OH,F)-rich spessartine (1)						
	U_{11}	U_{22}	U_{33}	U_{23}	U_{13}	U_{12}
Mn1	0.005 (1)	0.010 (1)	0.009 (1)	−0.002 (1)	0	0
Mn2	0.009 (1)	0.009 (1)	0.005 (1)	0	0	−0.002 (1)
Al	0.005 (1)	0.004 (1)	0.005 (1)	0.000 (1)	0.000 (1)	0.000 (1)
Si1	0.004 (1)	0.005 (1)	0.005 (1)	0.000 (1)	0	0
Si2	0.005 (1)	0.005 (1)	0.004 (1)	0	0	0
O1	0.007 (1)	0.006 (1)	0.006 (1)	−0.001 (1)	0.000 (1)	−0.001 (1)
O2	0.005 (1)	0.005 (1)	0.007 (1)	0.001 (1)	0.000 (1)	−0.001 (1)
O3	0.008 (1)	0.006 (1)	0.007 (1)	0.001 (1)	−0.001 (1)	0.000 (1)
O22	0.007 (1)	0.006 (2)	0.009 (1)	0.001 (1)	−0.001 (1)	0.000 (1)
F11	0.009 (2)	0.011 (2)	0.009 (1)	−0.002 (1)	0.000 (1)	−0.002 (1)
(*b*) Henritermierite (4)						
	U_{11}	U_{22}	U_{33}	U_{23}	U_{13}	U_{12}
Ca1	0.006 (1)	0.007 (1)	0.008 (1)	−0.001 (1)	0	0
Ca2	0.009 (1)	0.009 (1)	0.007 (1)	0	0	−0.003 (1)
Mn^{3+}	0.006 (1)	0.006 (1)	0.005 (1)	−0.001 (1)	−0.001 (1)	0.001 (1)
Si1	0.005 (1)	0.006 (1)	0.005 (1)	0.000 (1)	0	0
O1	0.010 (1)	0.007 (1)	0.006 (1)	−0.001 (1)	0.000 (1)	−0.001 (1)
O2	0.008 (1)	0.008 (1)	0.008 (1)	0.001 (1)	0.001 (1)	−0.002 (1)
O3	0.010 (1)	0.008 (1)	0.009 (1)	−0.001 (1)	0.003 (1)	−0.002 (1)

O22,F11⟩ = 1.847 (4) Å [Table 6(*a*)]. In spite of differences between this study, Boiocchi *et al.* (2012), and cubic spessartine, the mean ⟨D—O⟩ distances are similar. The lowering from cubic to tetragonal symmetry arises from ordering of [SiO_4] and [$(O_2H_2)F_2$] tetrahedra. A new possible end member for (OH,F)-spessartine is $^X Mn_3{}^Y Al_2{}^Z[(SiO_4)_2(O_2H_2)_{0.5}(F_2)_{0.5}]_{\Sigma3}$, which is unknown.

The bond-valence sums (BVS) indicate that the O3 site is nearly charge balanced [Tables 4(*a*) and 7(*a*)], but the O1 and O2 sites are under-bonded because they are part of split sites. The partially occupied F11 and O22 sites are under-bonded, indicating that these are monovalent F and OH anions, respectively. This is also confirmed from their s.o.f.s that agree with the chemical analysis. All the BVS for the cations are close to expected values [Table 7(*a*)].

Rhodochrosite, $MnCO_3$, is probably an original mineral from which (OH,F)-spessartine was formed as a hydrothermal reaction product that includes quartz, SiO_2, corundum, Al_2O_3, F_2 (or fluorite CaF_2), and H_2O. A possible reaction is:

$3MnCO_3 + Al_2O_3 + 2SiO_2 + 0.5F_2 + 0.5H_2O = Mn_3Al_2[(SiO_4)_2(O_2H_2)_{0.5}(F_2)_{0.5}]_{\Sigma3} + 3CO_2$.

4.2. Crystal structure of henritermierite

The chemical formula obtained using the EPMA for the henritermierite sample is $^X Ca_3{}^Y(Mn_{1.94}Al_{0.04}Fe_{0.02})_{\Sigma2}{}^Z[(SiO_4)_{1.98}(O_4H_4)_{1.02}]_{\Sigma3}$ (Table 1). The corresponding formula from the SCXRD structure refinement is $^X Ca_3{}^Y(Mn_{1.94}Al_{0.06})_{\Sigma2}{}^Z[(SiO_4)_{2.02}(O_4H_4)_1]_{\Sigma3}$, which is close to ideal formula $^X Ca_3{}^Y Mn_2{}^Z[(SiO_4)_2(O_4H_4)_1]_{\Sigma3}$

Table 6
Selected distances (Å) and angles (°).

(*a*) (OH,F)-rich spessartine

		(1) This study	(2) Boiocchi *et al.* (2012)		
Mn1—O1	×2	2.256 (1)	2.251 (1)		
Mn1—O2	×2	2.260 (3)	2.257 (1)		
Mn1—O2	×2	2.422 (3)	2.407 (1)		
Mn1—O3	×2	2.4148 (5)	2.418 (1)		
⟨Mn1—O⟩	[8]	2.338 (1)	2.333 (1)		
[Mn1—O22]	×2	2.173 (11)	–		
[Mn1—O22]	×2	2.315 (9)	–		
[Mn1—F11]	×2	2.173 (9)	–		
Mn2—O1	×4	2.411 (1)	2.416 (1)		
Mn2—O3	×4	2.2583 (5)	2.258 (1)		
⟨Mn2—O⟩	[8]	2.335 (1)	2.337 (1)		
⟨Mn1,2—O1,2,3⟩	[8]	2.336 (1)	2.335 (1)	⟨Mn—O⟩ [8]	2.3249 (2)
[Mn2—F11]	×4	2.269 (8)	–		
Al—O1	×2	1.906 (1)	1.896 (1)		
Al—O2	×2	1.902 (3)	1.901 (1)		
Al—O3	×2	1.8993 (5)	1.903 (1)		
⟨Al—O⟩	[6]	1.902 (1)	1.900 (1)	Al—O ×6	1.8956 (4)
[Al—O22]	×2	1.838 (10)	–		
[Al—F11]	×2	1.818 (8)	–		
Si1—O1	×2	1.6440 (9)	1.642 (1)		
Si1—O2	×2	1.633 (2)	1.645 (1)		
⟨Si1—O⟩	[4]	1.639 (1)	1.644 (1)		
Si1—O22	×2	1.815 (6)	–		
Si1—F11	×2	1.878 (5)	–		
⟨Si1—O22,F11⟩ = *Z*1□	[4]	1.847 (4)			
Si2—O3	×4	1.6427 (4)	1.634 (1)		
[Si2—O33]	×4	–	1.838 (4)		
⟨Si1,2—O1,2,3⟩		1.641 (1)	1.639 (1)	Si—O ×4	1.6416 (4)
⟨D—O⟩‡		2.054 (1)	2.052 (1)	⟨D—O⟩	2.0467 (2)
Al—O1—Si1	×1	133.22 (7)	133.4		
Al—O2—Si1	×1	133.7 (1)	133.2		
Al—O3—Si2	×1	133.45 (3)	133.6	Al—O—Si ×1	133.05 (2)
Al—O33—Si2	×1	–	125.1		

For henritermierite, a split O-atom site into O3 and O33 positions was used by Armbruster *et al.* (2001). The O33 site represents the O atom of the SiO_4 group. Δ = difference between Armbruster *et al.* (2001) and this study. There are no significant differences between these studies.

(*b*) Henritermierite

		(4) This study	(5) Armbruster *et al.* (2001)	Δ = (5) − (4)
Ca1—O1	×2	2.4773 (5)	2.476 (1)	−0.001
Ca1—O2	×2	2.4504 (5)	2.450 (1)	0.000
Ca1—O2	×2	2.4504 (5)	2.451 (1)	0.001
Ca1—O3	×2	2.4484 (6)	2.445 (1)	−0.003
⟨Ca1—O1,2,3⟩	[8]	2.4566 (3)	2.456 (1)	−0.001 (1)
[Ca1—O33]	×2	–	2.66 (3)	
Ca2—O1	×4	2.6157 (5)	2.614 (1)	−0.002
Ca2—O3	×4	2.3328 (5)	2.334 (1)	0.001
⟨Ca2—O1,3⟩	[8]	2.4743 (4)	2.474 (1)	0.000 (1)
[Ca2—O33]	×4	–	2.33 (3)	
⟨Ca1,Ca2—O1,2,3⟩		2.4654 (3)	2.465 (1)	0.000 (1)
Mn—O1	×2	1.9513 (5)	1.952 (1)	0.001
Mn—O2	×2	2.2068 (5)	2.206 (1)	−0.001
Mn—O3	×2	1.9075 (5)	1.904 (1)	−0.004
⟨Mn—O1,2,3⟩	[6]	2.0219 (3)	2.021 (1)	−0.001 (1)
[Mn—O33]	×2	–	2.04 (3)	

Table 6 (continued)

(*b*) Henritermierite

		(4) This study	(5) Armbruster *et al.* (2001)	Δ = (5) − (4)
Si1—O1	×2	1.6566 (5)	1.657 (1)	0.000
Si1—O2	×2	1.6297 (5)	1.630 (1)	0.000
⟨Si1—O1,2⟩	[4]	1.6432 (4)	1.644 (1)	0.001 (1)
Si2—O3 = *Z*2[]	×4	1.9773 (6)	1.982 (1)	0.005 (1)
[Si2—O33]	×4	–	1.70 (2)	
⟨Si1,2—O1,2,3⟩	×4	1.8102 (4)	1.813 (1)	0.003 (1)
⟨D—O⟩		2.1907 (2)	2.191 (1)	0.000 (1)
Mn—O1—Si1	×1	132.99 3)	–	
Mn—O2—Si1	×1	134.39 (3)	–	
Mn—O3—Si2	×1	125.86 (3)	–	
O3—H3	×1	0.73 (2)	0.75 (3)	0.02 (4)
Si2—H3	×1	1.64 (2)	–	
H3···O2	×1	2.198	2.21 (3)	0.01
O3—O2	×1	2.773	2.763 (1)	−0.010
O3—O3	×2	3.294	3.301 (1)	0.007
O3—O3	×1	3.094	3.095 (2)	0.001
O3—H3···O2	×1	136.4	134 (3)	−2
O3—H3—O3	×1	140.3	138 (3)	2

† The dominant anhydrous cubic $Ia\bar{3}d$ phase of a spessartine sample from California with a = 11.61332 (1) Å (Antao & Round, 2014). ‡ ⟨D—O⟩ = [⟨*X*1—O⟩ + ⟨*X*2—O⟩ + ⟨*Y*—O⟩ + mean of ⟨*Z*1—O⟩ and *Z*2—O3]/4. Split positions are O1 and F11 (O1—F11 = 0.249 Å) and O2 and O22 (O2—O22 = 0.200 Å) (this study), or O3 and O33 (O3—O33 = 0.22 Å; Boiocchi *et al.*, 2012).

Table 7
Bond-valence sums (v.u.)†.

(*a*) Obtained with SCXRD data for (1) (OH,F)-rich spessartine

	Si1	Si2	Mn1	Mn2	Al	Σ
O1	0.805 × 2		0.241 × 2	0.146 × 4	0.392 × 2	1.584
O2	0.751 × 2		0.216 × 2		0.359 × 2	
O2			0.139 × 2			1.465
O3		0.951 × 4	0.185 × 2	0.260 × 4	0.470 × 2	1.866
O22	0.137 × 2		0.082 × 2			
O22			0.056 × 2		0.127 × 2	0.402
F11	0.067 × 2		0.042 × 2	0.029 × 4	0.072 × 2	0.210
Σ	3.523	3.803	1.920	1.741	2.841	

(*b*) Henritermierite (4)

	Si1	Si2	Ca1	Ca2	Mn^{3+}	Σ
O1	0.888 × 2		0.244 × 2	0.168 × 4	0.569 × 2	1.869
O2	0.955 × 2		0.263 × 2		0.285 × 2	
			0.263 × 2			1.766
O3			0.264 × 2	0.361 × 4	0.641 × 2	1.266
H3≡O‡		≃ 0.9 × 4				
Σ	3.686	3.6	2.066	2.116	2.990	

† Brese & O'Keeffe (1991), Brown (2002). ‡ If an Si2 atom is present, the O atom may occupy the H3 position with O3 vacant, so each such O contributes ≃0.9 v.u. to Si2.

[Table 4(*b*)]. The agreement between EPMA and the SCXRD structure refinement results is reasonable (Table 1).

All the sites are fully occupied in henritermierite, except for the Si2 site that appears to be vacant [Table 4(*b*)]. The O3 and H3 sites are fully occupied, in contrast with the results from Armbruster *et al.* (2001) where the O3 position was split between an O3 position and a nearby O33 position. The U_{eq} for O3 is similar to those for O1 or O2, and that for the Si2 site

is large, indicating a vacant site as confirmed by the small s.o.f. value [Table 4(*b*)]. The unsplit O3 site together with the H3 atom describes the O_4H_4 groups (Fig. 6*d*). If the *Z*2 site is occupied with a Si atom, the O atom may occupy the H3 position with the O3 site vacant because *Z*2—H3 × 4 = 1.64 (2) Å is about the distance for the Si—O bond [Table 6(*b*)].

Our bond distances and angles are nearly identical to those obtained by Armbruster *et al.* (2001) if their O33 site is ignored [Table 6(*b*)]. The under-bonded O3 atom is charge balanced by forming a bond with an H atom where O3—H3 = 0.73 (2) Å [Tables 6(*b*) and 7(*b*)]. This distance is shorter than 1 Å that is expected for an O—H bond and is justified by the formation of the H3···O2 = 2.2 Å hydrogen bond [Figs. 6(*c*) and 6(*d*)]. The BVS indicates that O2 is under-bonded because of Mn—O2 Jahn–Teller elongation.

The two XO_8 dodecahedra have similar average ⟨Ca1—O⟩ = 2.4566 (3) Å and ⟨Ca2—O⟩ = 2.4743 (4) Å distances [Table 6(*b*)]. The average ⟨Ca1,Ca2—O⟩ = 2.4654 (3) Å distance is similar to ⟨Ca—O⟩ = 2.4517 (6) Å in cubic katoite, $(Ca_{2.95}Fe_{0.03})\{Al_{2.03}\}[(SiO_4)_{1.12}(O_4H_4)_{1.88}]$ (Ferro *et al.*, 2003). The average distances for henritermierite plot just to the right of katoite that contains a short O—H bond (see Fig. 7).

The MnO_6 octahedra contains Jahn–Teller distortions in henritermierite where the average ⟨Mn—O⟩ = 2.0219 (3) Å, but there is an elongation of Mn—O2 = 2.2068 (5) Å [Table 6(*b*); Fig. 6(*c*)]. This Jahn–Teller octahedral elongation is less than that in hausmannite spinel, $Mn^{2+}Mn^{3+}{}_2O_4$, from the Kalahari Manganese Field that has Mn^{3+}—O × 4 = 1.9276 (5) Å and Mn^{3+}—O × 2 = 2.2845 (8) Å, so the average ⟨Mn—O⟩ = 2.0466 (5) Å (our unpublished data) is larger than that for henritermierite.

The average ⟨Si1—O⟩ = 1.6432 (4) Å, which is the same as in many anhydrous cubic garnets with no significant Si-atom vacancies [*Z*—O horizontal line in Fig. 7; Table 6(*b*)]. The average ⟨*Z*2—O3⟩ = 1.9773 (6) Å indicates a vacant *Z*2 site, and the tetrahedron is made up of O_4H_4 [Figs. 6(*c*) and 6(*d*)]. The mean ⟨D—O⟩ = 2.1907 (2) Å is the same as that found previously. The lowering from cubic to tetragonal symmetry arises from ordering of $[SiO_4]$ and (O_4H_4) tetrahedra, which is triggered by O2—Mn^{3+}—O2 Jahn–Teller elongation (Armbruster *et al.*, 2001).

Hausmannite and henritermierite occur as an intergrowth, which is easily observed in BSE images (Fig. 8). Hausmannite is probably an original mineral from which henritermierite was formed by a reaction that includes quartz, SiO_2, calcite, $CaCO_3$ and H_2O. A possible reaction is:

$\frac{2}{3}Mn_3O_4 + 2SiO_2 + 3CaCO_3 + 2H_2O + 0.165O_2 = Ca_3Mn_2[(SiO_4)_2(O_4H_4)_1]_{\Sigma 3} + 3CO_2$.

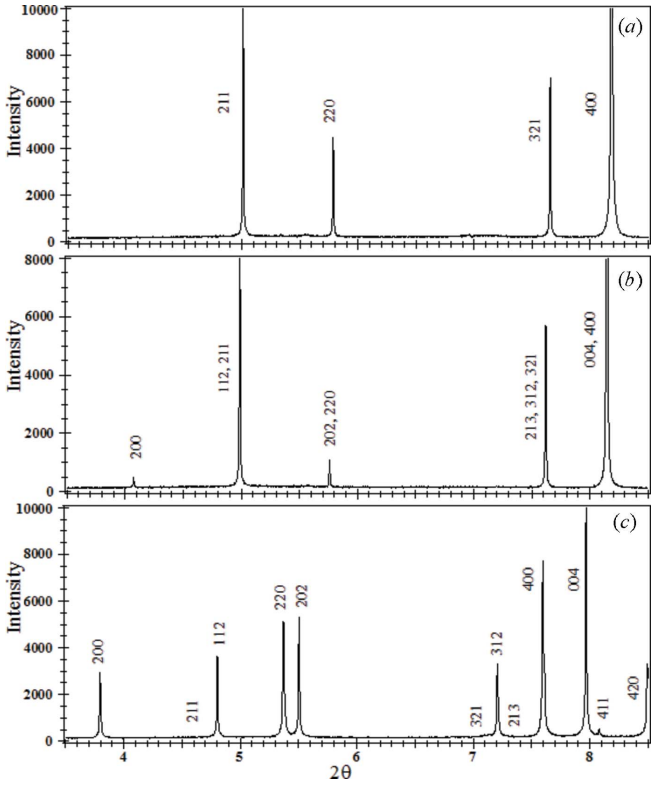

Figure 5
Comparison of experimental traces for (*a*) cubic ($Ia\bar{3}d$) spessartine from California (Antao & Round, 2014); (*b*) tetragonal ($I4_1/acd$) (OH,F)-spessartine; and (*c*) tetragonal ($I4_1/acd$) henritermierite. The 200 reflections is absent in (*a*) and is observed in the tetragonal garnets (*b*, *c*). The 200 reflection may be used to distinguish between tetragonal and cubic garnets.

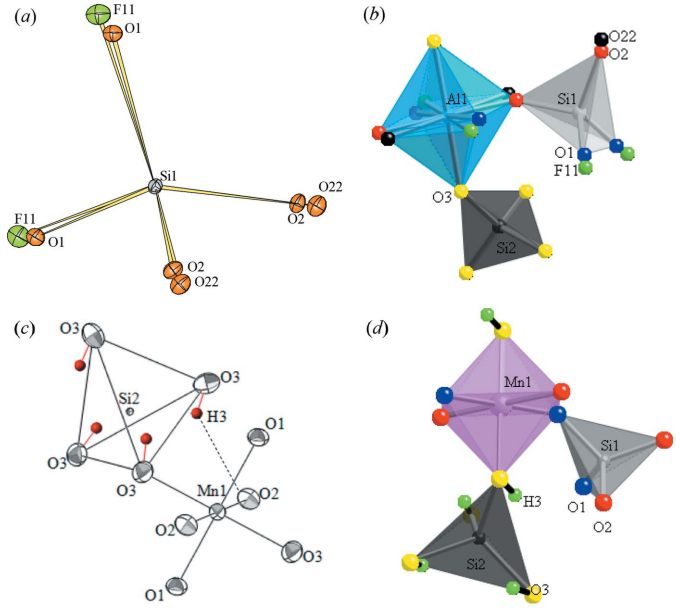

Figure 6
(*a*) Oxygen and fluorine atoms around the *Z*1 site in (OH,F)-spessartine. When the *Z*1 site is occupied, it is surrounded by 2 × O1 and 2 × O2 atoms. Each anion site is split. When the *Z*1 site is vacant, it is surrounded by 2 × F11 and 2 × O22 atoms, *i.e.* $[(O_2H_2)F_2]$ tetrahedron. (*b*) A *Y* octahedron, *Z*1 and *Z*2 tetrahedra in (OH,F)-spessartine. The *Z*2 site is fully occupied with Si atoms that bond to four O3 atoms. The *Z*1 tetrahedron is described in (*a*). (*c*) In henritermierite, the H atom bonds to the O3 atoms around the vacant *Z*2 site and forms a hydrogen bond to the O2 atom because of Jahn–Teller elongation along the O2—Mn^{3+}—O2 direction of the octahedron, which causes the O2 atom to be under-bonded [Table 7(*b*)]. (*d*) An octahedron and two tetrahedra around the *Y* and *Z* sites in henritermierite. The O3—H3 bond is shown with the H atoms just outside the faces of the *Z*2 tetrahedron.

Alternatively, henritermierite from the Kalahari Manganese Field was formed as a hydrothermal reaction product of the original braunite-rich manganese ores, $Mn^{2+}Mn_6^{3+}O_8[SiO_4]$ (Cairncross *et al.*, 1997). Similar formation conditions were proposed for henritermierite from Anti-Atlas, Morocco, where it is associated with marokite, $CaMn_2O_4$, hausmannite, and calcite (Gaudefroy *et al.*, 1969). A possible reaction with braunite is:

$2Mn^{2+}Mn_6^{3+}O_8[SiO_4] + 3CaCO_3 + 2H_2O = Ca_3Mn_2[(SiO_4)_2(O_4H_4)_1]_{\Sigma 3} + 4Mn_3O_4 + 3CO_2$.

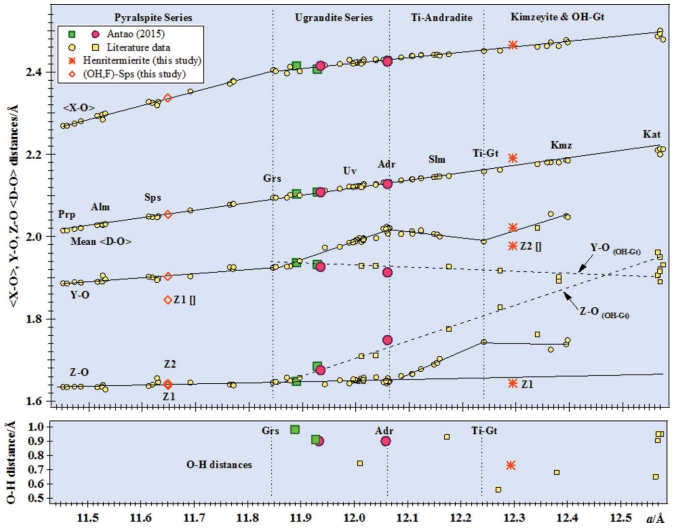

Figure 7
Structural variations in common garnets. Cubic hydrogarnet $Y-O_{(OH\text{-}Gt)}$ and $Z-O_{(OH\text{-}Gt)}$ dashed trend lines (arrows) extend from the maximum unit-cell parameter to end-member grossular (Grs). The hydrogarnet average $\langle X-O\rangle$ and mean $\langle D-O\rangle$ distances occur on the general solid trend lines for cubic anhydrous garnets. Known O—H distances are shown. For (OH,F)-spessartine and henritermierite, their average $\langle X-O\rangle$, $\langle Y-O\rangle$ and $\langle Z-O\rangle$ distances are shown in Table 6. These average distances fall on the respective trend lines. Two vacant Z site —O distances, labelled $Z1[]$ and $Z2[]$, are shown. The $Z2$ [] distance [1.9773 (6) Å] is larger than $Z-O = 1.828$ Å in cubic katoite garnet with $a = 12.270$ (1) Å, which is plotted just left to henritermierite (Ferro *et al.*, 2003).

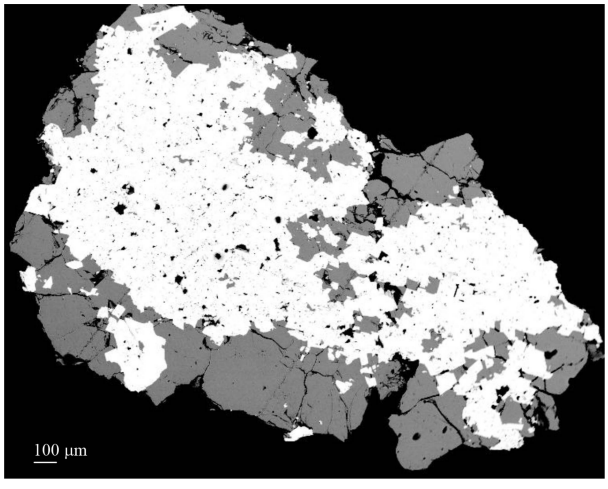

Figure 8
Intergrowth of henritermierite (dark grey) and hausmannite (white).

Crystal structure refinements show that cation vacancies occur in garnets and are well known in cubic hydrogarnets (*e.g.* Antao, 2015; Basso *et al.*, 1984*b*,*a*). Deficiencies in the s.o.f.s of Si (about 5–6%) may indicate minor substitution of (O_4H_4) for SiO_4 groups. If (O_4H_4) substitution occurs, then the s.o.f. of Z is < 1, and the unit-cell edge a increases, $Z-O$ increases and $Y-O$ decreases simultaneously from their corresponding values in the anhydrous cubic phase (Fig. 7; Antao, 2015).

Data from this study are inserted in Fig. 7, which shows the structural variations across the cubic garnet-group minerals, including cubic hydrogarnets (Antao, 2013*b*,*c*). The O—H distances are shown for the few samples where they are known. For the tetragonal garnets, all the average pseudo-cubic distances fall on the respective trend lines, except for the Z site that contains vacancies.

5. Conclusions

This study indicates that most common garnet-group minerals crystallize with cubic symmetry, but a few rare members crystallize with tetragonal symmetry. The tetragonal members are henritermierite, holtstamite and (OH,F)-rich spessartine. Their tetragonal symmetry arises mainly from OH^-, F^- and O^{2-} anion ordering. Although Y cations such as Mn^{3+} may trigger anion ordering through Jahn–Teller distortion, it is not a requirement in (OH,F)-rich spessartine. Tetragonal garnets contain OH^- and F^- anions, so they were probably formed at lower temperatures than garnets that contain only O^{2-} anions. Tetragonal garnets have distinct X-ray diffraction patterns that are different from cubic garnets. The reason for tetragonal majoritic-type garnets arising from Y cation ordering requires further investigation.

Acknowledgements

We thank the two anonymous referees and the co-editor, Simon Parsons, for useful comments that improved this manuscript. Benjamin Gelfand is thanked for his help with the single-crystal data collection. Robert Marr is thanked for his help with the electron probe. Jian Jun Li is thanked for his help with the FTIR measurement. The HRPXRD data were collected at the X-ray Operations and Research beamline 11-BM, Advanced Photon Source, Argonne National Laboratory.

Funding information

The following funding is acknowledged: US Department of Energy (contract No. DE-AC02-06CH11357). This work was supported with a NSERC Discovery Grant to SMA.

References

Akaogi, M. & Akimoto, S. (1977). *Phys. Earth Planet. Inter.* **15**, 90–106.
Akizuki, M. (1984). *Am. Mineral.* **66**, 403–409.
Allen, F. M. & Buseck, P. R. (1988). *Am. Mineral.* **73**, 568–584.

Angel, R., Finger, L. W., Hazen, R. M., Kanzaki, M., Weidner, D. J., Liebermann, R. C. & Veblen, D. R. (1989). *Am. Mineral.* **74**, 509–512.

Antao, S. M. (2013*a*). *Can. Mineral.* **51**, 771–784.

Antao, S. M. (2013*b*). *Phys. Chem. Miner.* **40**, 705–716.

Antao, S. M. (2013*c*). *Powder Diffr.* **28**, 281–288.

Antao, S. M. (2014*a*). *Powder Diffr.* **29**, 325–330.

Antao, S. M. (2014*b*). *Powder Diffr.* **29**, 346–351.

Antao, S. M. (2015). *Phys. Chem. Miner.* **42**, 455–474.

Antao, S. M. & Cruickshank, L. A. (2016). *Acta Cryst.* B**72**, 846–854.

Antao, S. M., Duane, M. J. & Hassan, I. (2002). *Can. Mineral.* **40**, 1403–1409.

Antao, S. M. & Hassan, I. (2002). *Can. Mineral.* **40**, 163–172.

Antao, S. M. & Hassan, I. (2010). *Can. Mineral.* **48**, 1217–1223.

Antao, S. M. & Klincker, A. M. (2013). *Phys. Chem. Miner.* **40**, 575–586.

Antao, S. M. & Klincker, A. M. (2014). *Powder Diffr.* **29**, 20–27.

Antao, S. M., Mohib, S., Zaman, M. & Marr, R. A. (2015). *Can. Mineral.* **53**, 133–158.

Antao, S. M. & Round, S. A. (2014). *Powder Diffr.* **29**, 233–240.

Antao, S. M., Suarez Nieto, N. S., Cruickshank, L. A. & Gwanmesia, G. D. (2015). *Adv. X-ray Anal.* **59**, 192–211.

Antao, S. M., Zaman, M., Gontijo, V. L., Camargo, E. S. & Marr, R. A. (2015). *Contrib. Mineral. Petrol.* **169**, 10.

Antao, S. M., Zaman, M., Suarez Nieto, N. S., Gontijo, V. L. & Marr, R. A. (2014). *Adv. X-ray Anal.* **58**, 90–107.

Armbruster, T. (1995). *Eur. J. Mineral.* **7**, 1221–1225.

Armbruster, T., Kohler, T., Libowitzky, E., Friedrich, A., Miletich, R., Kunz, M., Medenbach, O. & Gutzmer, J. (2001). *Am. Mineral.* **86**, 147–158.

Aubry, A., Dusausoy, Y., Laffaille, A. & Protas, J. (1969). *Bull. Soc. Fr. Mineral.* **92**, 126–133.

Bank, H. (1982). *Z. Dtsch. Gemmologischen Ges.* **31**, 93–96.

Basso, R., Cimmino, F. & Messiga, B. (1984*a*). *Neues Jahrb. Mineral. Abh.* **148**, 246–258.

Basso, R., Cimmino, F. & Messiga, B. (1984*b*). *Neues Jahrb. Mineral. Abh.* **150**, 247–258.

Boiocchi, M., Bellatreccia, F., Della Ventura, G. D. & Oberti, R. (2012). *Z. Kristallogr.* **227**, 385–395.

Brese, N. E. & O'Keeffe, M. (1991). *Acta Cryst.* B**47**, 192–197.

Brewster, D. (1853). *Philos. Mag. Ser.* 4, **6**, 16–30.

Brown, I. D. (2002). *The Chemical Bond in Inorganic Chemistry. The Bond Valence Model*. Oxford University Press.

Brown, D. & Mason, R. A. (1994). *Can. Mineral.* **32**, 105–110.

Caglioti, G., Paoletti, A. & Ricci, F. P. (1958). *Nucl. Instrum.* **3**, 223–228.

Cairncross, B., Beukes, N. & Gutzmer, J. (1997). *The Manganese Adventure; The South African Manganese Fields. Associated Ore and Metal Cooperation Limited*. p. 236. Marshalltown, Johannesburg, Republic of South Africa.

Deer, W. A., Howie, R. A. & Zussman, J. (1982). *Orthosilicates*, Vol. 1A. New York: Longman Group Limited.

Ehm, L., Antao, S. M., Chen, J. H., Locke, D. R., Michel, F. M., Martin, C. D., Yu, T., Parise, J. B., Lee, P. L., Chupas, P. J., Shastri, S. D. & Guo, Q. Z. (2007). *Powder Diffr.* **22**, 108–112.

Farrugia, L. J. (2012). *J. Appl. Cryst.* **45**, 849–854.

Ferro, O., Galli, E., Papp, G., Quartieri, S., Szakáll, S. & Vezzalini, G. (2003). *Eur. J. Miner.* **15**, 419–426.

Frank-Kamenetskaya, O. V., Rozhdestvenskaya, L. V., Shtukenberg, A. G., Bannova, I. I. & Skalkina, Y. A. (2007). *Struct. Chem.* **18**, 493–503.

Fujino, K., Momoi, H., Sawamoto, H. & Kumazawa, M. (1986). *Am. Mineral.* **71**, 781–785.

Gaudefroy, C., Orliac, M., Permingeat, F. & Parenoff, E. (1969). *Bull. Soc. Fr. Minéral. Cristallogr.* **92**, 185–190.

Hålenius, U., Häussermann, U. & Harryson, H. (2005). *Eur. J. Mineral.* **17**, 375–382.

Hatch, D. M. & Ghose, S. (1989). *Am. Mineral.* **74**, 1221–1224.

Hatch, D. M. & Griffen, D. T. (1989). *Am. Mineral.* **74**, 151–159.

Heinemann, S., Sharp, T. G., Seifert, F. & Rubie, D. C. (1997). *Phys. Chem. Miner.* **24**, 206–221.

Hirai, H. & Nakazawa, H. (1986*a*). *Am. Mineral.* **71**, 123–126.

Hirai, H. & Nakazawa, H. (1986*b*). *Am. Mineral.* **71**, 1210–1213.

Ito, E. & Takahashi, E. (1987). In *High Pressure Research in Mineral Physics: A Volume in Honor of Syun-iti Akimoto*, edited by M. H. Manghnani & Y. Syono. *Geophys. Monogr.* **39**, 221–229.

Ivanova, T. I., Shtukenberg, A. G., Punin, Y. O., Frank-Kamenetskaya, O. V. & Sokolov, P. B. (1998). **62**, 857–868.

Jamtveit, B. (1991). *Am. Mineral.* **76**, 1319–1327.

Kato, T. & Kumazawa, M. (1985). *Nature*, **316**, 803–805.

Koritnig, S., Rösch, H., Schneider, A. & Seifert, F. (1978). *TMPM Tschermaks Petr. Mitt.* **25**, 305–313.

Larson, A. C. & Von Dreele, R. B. (2000). Report LAUR 86-748. Los Alamos National Laboratory, NM, USA.

Lee, P. L., Shu, D., Ramanathan, M., Preissner, C., Wang, J., Beno, M. A., Von Dreele, R. B., Ribaud, L., Kurtz, C., Antao, S. M., Jiao, X. & Toby, B. H. (2008). *J. Synchrotron Rad.* **15**, 427–432.

Liu, L. (1977). *Earth Planet. Sci. Lett.* **36**, 237–245.

Mallard, E. (1876). *Ann. Mines. Mem. VII Ser.* **10**, 60.

Manning, P. G. & Owens, D. R. (1977). *Can. Mineral.* **15**, 512–517.

Merli, M., Callegari, A., Cannillo, E., Caucia, F., Leona, M., Oberti, R. & Ungaretti, L. (1995). *Eur. J. Mineral.* **7**, 1239–1249.

Moyer, R. O., Antao, S. M., Toby, B. H., Morin, F. G. & Gilson, D. F. R. (2008). *J. Alloys Compd.* **460**, 138–141.

Nakatsuka, A. (2005). *Am. Mineral.* **90**, 755–757.

Nakatsuka, A., Yoshiasa, A., Takamitsu, Y., Osamu, O., Tomoo, K. & Ito, E. (1999). *Am. Mineral.* **84**, 1135–1143.

Nakatsuka, A., Yoshiasa, A., Yamanaka, T. & Ito, E. (1999). *Am. Mineral.* **84**, 199–202.

Novak, G. A. & Gibbs, G. V. (1971). *Am. Mineral.* **56**, 1769–1780.

Otwinowski, Z. & Minor, W. (1997). *Methods Enzymol.* **276**, 307–326.

Parise, J. B., Wang, Y., Gwanmesia, G. D., Zhang, J., Sinelnikov, Y., Chmielowski, J., Weidner, D. J. & Liebermann, R. C. (1996). *Geophys. Res. Lett.* **23**, 3799–3802.

Pollok, K., Jamtveit, B. & Putnis, A. (2001). *Contrib. Mineral. Petrol.* **141**, 358–366.

Prewitt, C. T. & Sleight, A. W. (1969). *Science*, **163**, 386–387.

Rietveld, H. M. (1969). *J. Appl. Cryst.* **2**, 65–71.

Ringwood, A. E. (1967). *Earth Planet. Sci. Lett.* **2**, 255–263.

Rossman, G. R. & Aines, R. D. (1991). *Am. Mineral.* **76**, 1153–1164.

Sawamoto, H. (1987). *In High Pressure Research in Mineral Physics: A Volume in Honor of Syun-iti Akimoto*, edited by M. H. Manghnani & Y. Syono. *Geophys. Monogr.* **39**, 209–219.

Schingaro, E., Lacalamita, M., Mesto, E., Ventruti, G., Pedrazzi, G., Ottolini, L. & Scordari, F. (2016). *Am. Mineral.* **101**, 371–384.

Sheldrick, G. M. (2015). *Acta Cryst.* C**71**, 3–8.

Skinner, L. B., Benmore, C. J., Antao, S. M., Soignard, E., Amin, S. A., Bychkov, E., Rissi, E., Parise, J. B. & Yarger, J. L. (2012). *J. Phys. Chem. C*, **116**, 2212–2217.

Smyth, J. R., Madel, R. E., McCormick, T. C., Munoz, J. L. & Rossman, G. R. (1990). *Am. Mineral.* **75**, 314–318.

Takéuchi, Y., Haga, N., Umizu, S. & Sato, G. (1982). *Z. Kristallogr.* **158**, 53–99.

Thompson, P., Cox, D. E. & Hastings, J. B. (1987). *J. Appl. Cryst.* **20**, 79–83.

Toby, B. H. (2001). *J. Appl. Cryst.* **34**, 210–213.

Ungaretti, L., Leona, M., Merli, M. & Oberti, R. (1995). *Eur. J. Mineral.* **7**, 1299–1312.

Wang, J., Toby, B. H., Lee, P. L., Ribaud, L., Antao, S. M., Kurtz, C., Ramanathan, M., Von Dreele, R. B. & Beno, M. A. (2008). *Rev. Sci. Instrum.* **79**, 085105.

Zabinski, W. (1966). *Pol. Akad. Nauk Oddzial Krakowie Kom. Nauk Mineral. Pr. Mineral.* **3**, 1–69.